Effects of superimposed hydrostatic pressure on fracture in round bars under tension

J. Peng [a], P.D. Wu [a,*], Y. Huang [b], X.X. Chen [a], D.J. Lloyd [c], J.D. Embury [d], K.W. Neale [e]

[a] Department of Mechanical Engineering, McMaster University, Hamilton, Ont., Canada L8S 4L7
[b] Departments of Civil and Environmental Engineering and Mechanical Engineering, Northwestern University, Evanston, IL 60208, USA
[c] Novelis Global Technology Centre, 945 Princess Street, Kingston, Ont., Canada K7L 5L9
[d] Department of Materials Science and Engineering, McMaster University, Hamilton, Ont., Canada L8S 4L7
[e] Faculty of Engineering, University of Sherbrooke, Sherbrooke, Que., Canada J1K 2R1

ARTICLE INFO

ABSTRACT

The effect of superimposed hydrostatic pressure on fracture in round bars under tension is studied numerically using the finite element method based on the Gurson damage model. It is demonstrated that while the superimposed hydrostatic pressure has no noticeable effect on necking, it increases the fracture strain due to the fact that a superimposed pressure delays or completely eliminates the nucleation, growth and coalescence of microvoids or microcracks. The experimentally observed transition of the fracture surface, from the cup-cone mode under atmospheric pressure to a slant structure under high pressure, is numerically reproduced. It is numerically proved that the superimposed hydrostatic pressure has no effect on necking for a damage-free round bar under tension.

1. Introduction

In the study of tensile fracture of 1045 spheroidized steel under hydrostatic pressure, Kao et al. (1990) characterized void formation in the tensile test under pressure through quantitative metallography, and analyzed the fracture mechanism under pressure in terms of fractography. Kao et al. (1990) clearly demonstrated that the influence of superimposed hydrostatic pressure on tensile fracture of 1045 spheroidized steel was such that void nucleation is suppressed, leading to larger post-uniform strains under pressure and a transition of the fracture surface from the cup-cone mode under atmospheric pressure to a slant structure under high pressure (see Fig. 1). The work by Kao et al. (1990) further supported the general trend: increasing pressure leads to a significant increase in ductility and slight increase in flow stress.

In general, how superimposed hydrostatic pressure affects the mechanical behavior of various different engineering materials and their composites has been extensively investigated (see e.g. Sauer et al., 1970; French et al., 1973; French and Weinrich, 1975; Weinrich and French, 1976; Brownrigg et al., 1983; Korbel et al., 1984; Spitzig and Richmond, 1984; Ashby et al., 1985; Kao et al., 1989, 1990; Liu and Lewandowski, 1993). Most of these works were comprehensively reviewed by Lewandowski and Lowhaphandu (1998). It has been generally accepted that superim-

posed hydrostatic pressure increases the ductility of sheet metals due to the fact that a superimposed pressure delays or completely eliminates the nucleation, growth and coalescence of microvoids or microcracks (see e.g. Gimple et al., 2001).

Very recently, Wu et al. (2009) have studied effects of superimposed hydrostatic pressure on sheet metal formability. The effect of superimposed hydrostatic pressure was included in the analysis of the forming limit diagram for sheet metals. It has been observed that the superimposed hydrostatic pressure increases sheet metal limit strains for any strain path. However, the analyses carried out by Wu et al. (2009) underestimate the effect of superimposed hydrostatic pressure on formability/ductility of sheet metals because their analysis was based on the classic isotropic rate-independent plasticity theory, in which the damage effect due to void nucleation and growth was completely ignored. Without going to any details, Wu et al. (2009) have also numerically demonstrated the experimentally observed transition of the fracture surface, from the cup-cone mode under atmospheric pressure to a slant structure under high pressure.

The purpose of this paper is to carry out a detailed numerical study of the influence of superimposed hydrostatic pressure on fracture in round bars under tension. It is noted that Tvergaard and Needleman (1984) have successfully studied the cup-cone fracture in a round tensile bar at room pressure. However, to the best of our knowledge, the effects of superimposed hydrostatic pressure on fracture in a round tensile bar have not been numerically studied. All simulations reported in the present paper are

---

* Corresponding author. Tel.: +1 905 525 9140x20092; fax: +1 905 572 7944.
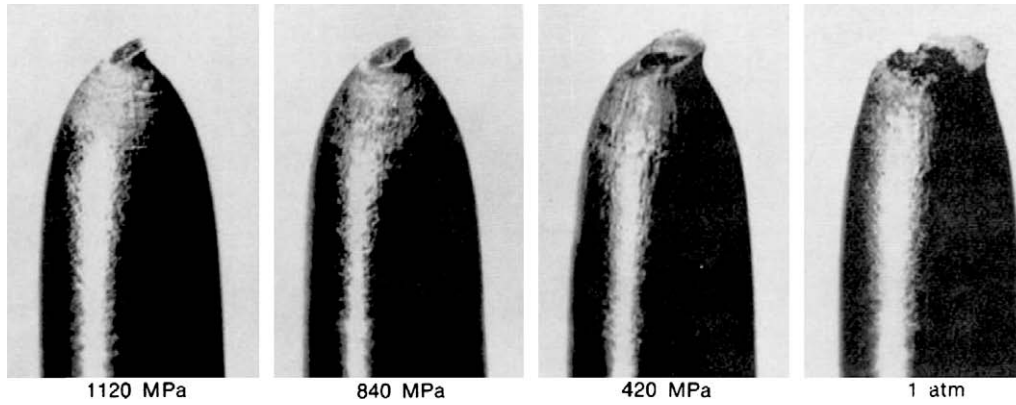 E-mail address: peidong@mcmaster.ca (P.D. Wu).

Fig. 1. The appearance of the fractured tensile bars under applied pressure (from Kao et al., 1990).

performed using ABAQUS and the mechanical behavior of the round bars are characterized by the Gurson damage model (Gurson, 1977; Tvergaard, 1990). Numerical results are found to be in good agreement with experimental observations found in the literature. It is also demonstrated numerically that a superimposed hydrostatic pressure has no effect on the uniform strain for damage free materials.

2. Constitutive model

Gurson (1977) proposed a yield function of the form $\phi(\sigma, \bar{\sigma}, f)$ for a porous plastic solid with a randomly distributed volume fraction, f, of voids. Here, σ is the macroscopic Cauchy stress tensor and $\bar{\sigma}$ is the matrix flow strength. The original Gurson model has been improved significantly (see e.g. Chu and Needleman, 1980; Tvergaard, 1981, 1982; Mear and Hutchinson, 1985; Chen et al., 2004; Nahshon and Hutchinson, 2008). The approximate yield function to be used in this paper is of the form

$$\phi(\sigma, \bar{\sigma}, f) = \frac{\sigma_e^2}{\bar{\sigma}^2} + 2f^* q_1 \cosh\left(\frac{3q_2\sigma_H}{2\bar{\sigma}}\right) - \left[1 + (q_2 f^*)^2\right] = 0 \tag{1}$$

where the parameters q_1 and q_2 are calibration coefficients introduced by Tvergaard (1981) to improve the agreement with numerical studies of materials containing periodically distributed circular cylindrical or spherical voids. The function $f^*(f)$ was introduced by Tvergaard and Needleman (1984) to model the loss of stress carrying capacity accompanying void coalescence, such that

$$f^* = \begin{cases} f, & \text{for } f \leqslant f_c \\ f_c + \frac{f_u^* - f_c}{f_f - f_c}(f - f_c), & \text{for } f > f_c \end{cases} \tag{2}$$

where f_c is the porosity level at which void coalescence commences and f_f is the porosity level at final fracture. The parameter $f_u^* = 1/q_1$ is defined so that when $f = f_f$ the material has experienced a complete loss of strength.

The evolution of void volume fraction is due to the growth of existing voids and the nucleation of new voids:

$$\dot{f} = (\dot{f})_{\text{growth}} + (\dot{f})_{\text{nucleation}} \tag{3}$$

with the growth being a function of the plastic strain rate $\boldsymbol{D}^p$

$$(\dot{f})_{\text{growth}} = (1-f)\boldsymbol{I} : \boldsymbol{D}^p \tag{4}$$

and the nucleation according to

$$(\dot{f})_{\text{nucleation}} = \bar{A}\dot{\bar{\varepsilon}}^p \tag{5}$$

The parameter $\bar{A}$ is chosen so that nucleation follows a normal distribution as suggested by Chu and Needleman (1980):

$$\bar{A} = \frac{f_N}{s_N\sqrt{2\pi}} \exp\left[-\frac{1}{2}\left(\frac{\bar{\varepsilon}^p - \varepsilon_N}{s_N}\right)^2\right] \tag{6}$$

Here, ε_N is the average void nucleating strain, f_N is the volume fraction of void nucleating particles, s_N is the standard deviation of void nucleating strain. It is noted that voids are nucleated only in tension; ABAQUS will not consider the nucleation term at a material point if the stress state is compressive ($\sigma_H < 0$). The condition for nucleation (6) may lead to discontinuous results in cases where pressure is equal to 0. In that case an infinitesimal variation of pressure ($d\sigma_H$) may result in a finite variation of the nucleation rate if $d\sigma_H > 0$.

The uniaxial true stress–true strain curve for the matrix material is described by the following power-law form:

$$\bar{\varepsilon} = \begin{cases} \frac{\bar{\sigma}}{E}, & \text{for } \bar{\sigma} \leqslant \sigma_y \\ \frac{\sigma_y}{E}\left(\frac{\bar{\sigma}}{\sigma_y}\right)^n, & \text{for } \bar{\sigma} > \sigma_y \end{cases} \tag{7}$$

where σ_y is the yield stress, and n is the strain hardening exponent.

3. Problem formulation and method of solution

Mechanical testing with a superimposed hydrostatic pressure has generally been conducted on similar devices (see e.g. Lewandowski and Lowhaphandu, 1998). The specimen is inserted into the load train assembly present in a pressure vessel. Following pressurization of the fluid, the subsequent tension testing of the specimen is conducted at the desired level of superimposed hydrostatic pressure.

We consider a round tensile bar, with initial length $2L_0$ and initial radius R_0, under superimposed hydrostatic pressure as shown in Fig. 2. Due to the symmetry, only half of the tensile bar is investigated. More specifically, $Z = 0$ is a symmetric plane, and a tensile displacement is applied at $Z = L_0$. We further assume that $Z = L_0$ is a shear-free end.

The sequence of uniaxial tension under superimposed hydrostatic pressure is modelled as a two-step process. The first step is pressurization (Fig. 2a). During this step the pressure fluid has access to all surfaces of the specimen, and the magnitude of the pressure is gradually increased up to a desired level $p = -\alpha\sigma_y$ with α being a positive constant. The second step is to apply a tensile displacement at $Z = L_0$ at the desired level of superimposed hydrostatic pressure $p = -\alpha\sigma_y$ (Fig. 2b). To trigger necking at the middle-plane $Z = 0$, a small initial thickness inhomogeneity ΔR is assumed in the form of

$$\Delta R = -\xi R_0 \cos\left(\frac{\pi Z}{L_0}\right) \tag{8}$$
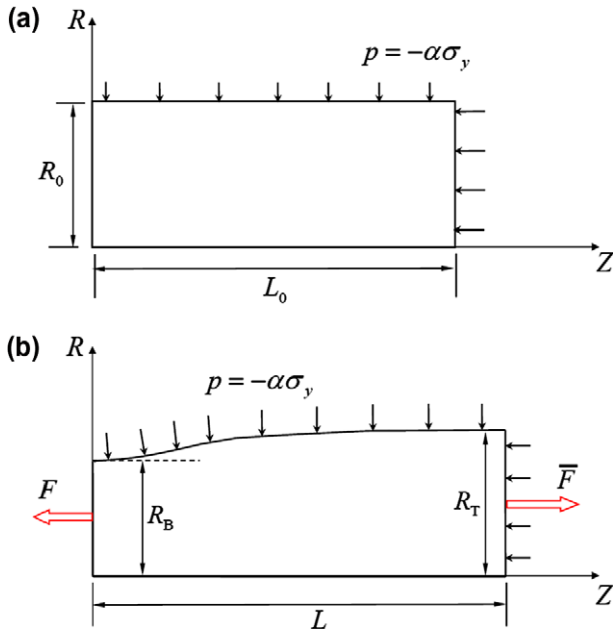
Fig. 2. Schematic representation of a round tensile bar under superimposed hydrostatic pressure (a) after pressurized to a desired level of pressure $p = -\alpha\sigma_y$, and (b) elongated in the axial direction under the desired pressure $p = -\alpha\sigma_y$.

Fig. 3. Mesh A with 28×42 quadrilateral elements (28 in the radius direction and 42 in the axial direction), each built up with four linear triangular elements (CAX3 in ABAQUS/Explicit).

It is important to note that in mechanical testing with superimposed hydrostatic pressure, the use of external load cells may produce erroneous data for the load required to deform the specimen because of a variable amount of seal friction which results during the pressurization in the vessel. In order to more accurately measure the load on the specimen inside the vessel, pressure compensated load cells consisting of a measuring load cell and a compensating load cell have been developed (see Carpentier and Contre, 1970). Before fracture occurs, from Fig. 2b, we have

$$\overline{F} - \alpha\sigma_y\left(\pi R_T^2\right) = F - \alpha\sigma_y\left(\pi R_T^2 - \pi R_B^2\right)$$

or

$$\overline{F} = F + \alpha\sigma_y\pi R_B^2 \qquad (9)$$

Note that πR_T^2 and πR_B^2 are the cross-sectional areas of the planes at $Z = L_0$ and $Z = 0$, respectively (see Fig. 2b). The above equation describes the relationship between the internal force F and applied force $\overline{F}$ under the *superimposed hydrostatic pressure* $p = -\alpha\sigma_y$.

It is important to point out that it is the applied load $\overline{F}$ and displacement ΔL curve that is converted into the true stress and true strain curves using Bridgman's (1952) correction factor based on the neck radius and neck profile radius during necking development. It should be noted that both F and $\overline{F}$ are normalized by $\sigma_y\pi R_0^2$ when they are plotted in figures shown in next section.

4. Results and discussion

4.1. Effects of superimposed hydrostatic pressure on necking in damage-free materials

We would like to start with assessing the effects of superimposed hydrostatic pressure on necking in damage-free round tensile bars.

It has been documented that, for most monolithic metals, a superimposed hydrostatic pressure significantly increases the fracture strain but has no noticeable effect on the uniform strain or necking strain (see e.g. Lewandowski and Lowhaphandu, 1998). The uniform strain is the strain at which diffuse necking is initiated. In an attempt to assess the effect of superimposed hydrostatic
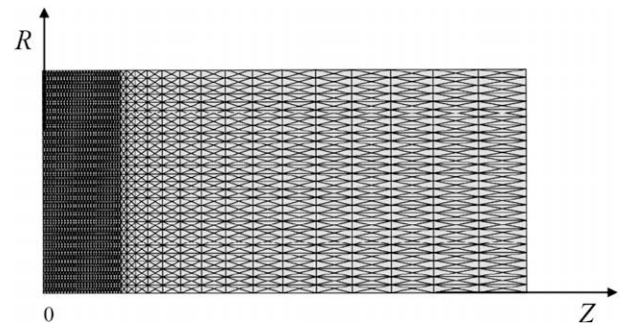
pressure on uniform strain for damage free metals, Wu et al. (2009) developed a Considère-type criterion to determine the onset of inhomogeneous deformation. They stated that such a criterion should be based on the condition of $dF = 0$ (rather than $d\overline{F} = 0$). Apparently, it is very difficult to mathematically prove that $dF = 0$ is more appropriate than $d\overline{F} = 0$ for determining the onset of necking and vice verse. However, this assessment can be done numerically. All simulations reported in Section 4.1 assume that there is neither initial void nor void nucleation, so that the Gurson model in (1) reduces to the classical von Mises plasticity theory, which was used in Wu et al. (2009). More specifically, the elastic–plastic properties of the damage-free round tensile bars are specified by $\sigma_y = 1$ MPa, $\sigma_y/E = 0.0033$, $v = 0.3$ and $n = 10$. We further assume that the initial length to radius ratio is given by $L_0/R_0 = 2$, and the value of the initial imperfection in (8) is assumed to be $\xi = 0.001$. In this classical necking problem, numerical results will not be very sensitive to a mesh used. We use a mesh, Mesh A as shown in Fig. 3, with local refinement around the middle-plane, and with total of 28×42 quadrilateral elements (28 in the radius direction and 42 in the axial direction), each built up with four linear triangular elements (CAX3 in ABAQUS/Explicit).

Fig. 4 shows the calculated internal force F and axial strain ε curves under different superimposed hydrostatic pressures. It is found that the strain at which the internal force F reaches its
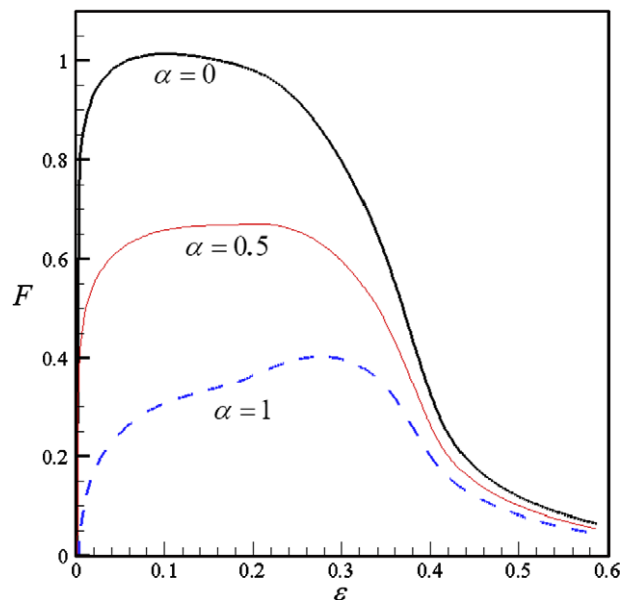

Fig. 4. Predicted *internal/net* force F and tensile strain $\varepsilon = \ln(1 + \Delta L/L_0)$ curves for the a damage free round bar under superimposed hydrostatic pressure $p = -\alpha\sigma_y$.
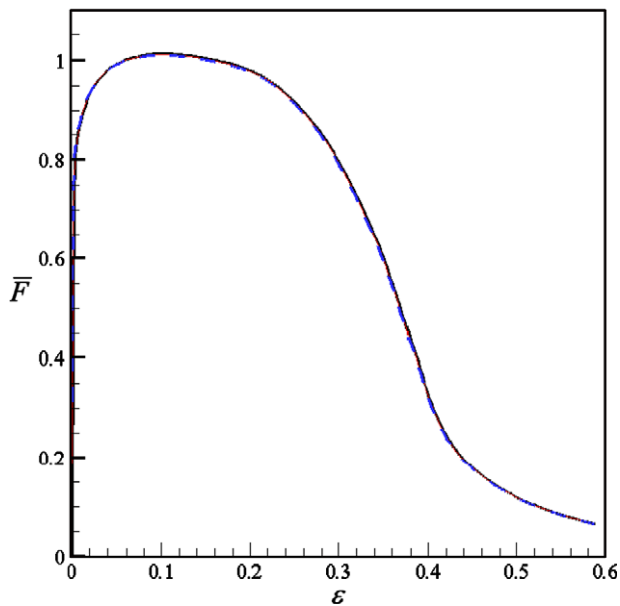
Fig. 5. Predicted *applied* force $\overline{F}$ and tensile strain $\varepsilon = \ln(1 + \Delta L/L_0)$ curves for a damage free round bar under superimposed hydrostatic pressure $p = -\alpha\sigma_y$.

maximum increases with increasing pressure. This would imply that the superimposed hydrostatic pressure could delay necking if the condition $dF = 0$ was used to define the onset of necking. Using (9), the $F-\varepsilon$ curves in Fig. 4 are converted into the $\overline{F}-\varepsilon$ curves in Fig. 5. It is found that the $\overline{F}-\varepsilon$ curves in Fig. 5 are actually identical. It is worthwhile to point out that the $\overline{F}-\varepsilon$ curves converted from the $F-\varepsilon$ curves according to (9) are identical to those directly calculated from the reaction force at $Z = L_0$. This implies that the round tensile bar is truly under the superimposed hydrostatic pressure during the entire uniaxial tension process. From Fig. 5, one would conclude that the superimposed hydrostatic pressure could have no effect on the uniform strain if $d\overline{F} = 0$ was used to define the onset of necking. The onset of necking and its evolution could be best presented in terms of the minimum radius $R_{\min}$ and axial strain ε curves, which are now shown in Fig. 6. It is clear that the calculated
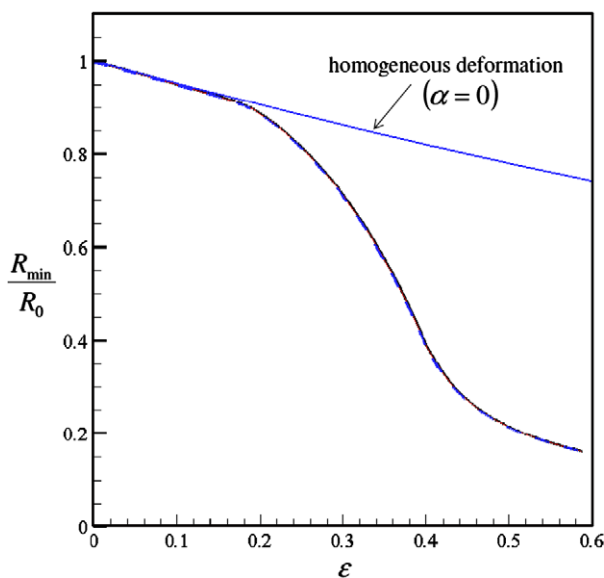

Fig. 6. Predicted normalized minimum radius $(R_{\min}/R_0)$ and tensile strain $\varepsilon = \ln(1 + \Delta L/L_0)$ curves for a damage free round bar under superimposed hydrostatic pressure $p = -\alpha\sigma_y$.

minimum radius $R_{\min}$ and axial strain ε curves under different superimposed hydrostatic pressures are identical. Examining deformed meshes at the same strain levels indicate that the necking profiles under different superimposed hydrostatic pressures are also identical. It thus becomes clear that the superimposed hydrostatic pressure has no effect on necking for damage free materials, and that $d\overline{F} = 0$ is appropriate to define the onset of necking.

4.2. Effects of superimposed hydrostatic pressure on fracture in porous materials

We now proceed by considering round tensile bars made of a porous material, which is described by the Gurson model. The elastic–plastic properties of the matrix material are specified by $\sigma_y = 1$ MPa, $\sigma_y/E = 0.0033$, $\nu = 0.3$ and $n = 10$. We assume that there are no initial voids, and the parameters $q_1 = 1.0$ and $q_2 = 1.5$ are used in the yield function (1). The void nucleation is assumed to be plastic strain controlled, with the volume fraction $f_N = 0.04$ of void nucleating particles, the mean strain for nucleation $\varepsilon_N = 0.3$, and the corresponding standard deviation $s_N = 0.1$. The final failure is taken to be characterized by the parameters $f_c = 0.15$ and $f_f = 0.25$. Similar to the damage-free round tensile bars, the initial length to radius ratio is given by $L_0/R_0 = 2$, and the value of the initial imperfection in (8) is assumed to be $\xi = 0.001$. It is important to point out that these values of the geometrical and material parameters are the same as those used in Tvergaard and Needleman (1984).

Significant mesh sensitivity is usually expected in a numerical simulation involving deformation localization and failure. For the problem considered in the present paper, as already mentioned by Tvergaard and Needleman (1984), the initial mesh design required for an analysis of final failure in a round tensile bar is essentially controlled by the first occurrence of fracture in the centre of the neck. Since Tvergaard and Needleman (1984) have carefully studied the mesh sensitivity in their analysis of the cup-cone fracture in a round tensile bar, we start with Mesh A (already shown in Fig. 3), which is very similar to the one used in Tvergaard and Needleman (1984). A finer mesh, Mesh B, consisting of 56×84 quadrilateral elements (56 in the radius direction and 84 in the axial direction) with local refinement near the middle-plane, is also used in the present work but mainly for the mesh sensitivity study.

We first consider the round tensile bar under uniaxial tension without a superimposed hydrostatic pressure $(p = 0)$. It is important to bear in mind that the main purpose of the present study is to assess the effects of superimposed pressure on fracture in a round tensile bar. Since the geometry and the values of the material parameters are exactly same as in Tvergaard and Needleman (1984), we only briefly explain how the cup-cone fracture surface is formed in a round tensile bar without superimposed hydrostatic pressure. For details, we refer to Tvergaard and Needleman (1984).

Fig. 7 presents the calculated tensile force F as a function of the tensile true strain $\varepsilon = \ln(1 + \Delta L/L_0)$, where ΔL is the displacement. For a comparison, the results based on homogeneous deformation are also included. It is found that the force increases linearly with the imposed straining when the deformation is very small and the material is essentially in the elastic state. With continued straining, the force gradually reaches its maximum at around $\varepsilon = 0.1$ and then gradually decreases due to both the reduction of the cross-sectional area and the softening effect resulting from void nucleation and growth. Further straining results in a sharp "knee" on the force and axial strain curve, which is associated with reaching the critical value of the void volume fraction $(f_c = 0.15)$ in the centre of the neck. Immediately after the sharp knee, the burst of void nucleation and growth leads to a rapid drop in true stress which in turn results in a rapid lose of load carry capacity for the tensile bar. From Fig. 7, it is clear that necking and failure in the fine mesh (Mesh B) occur earlier than those
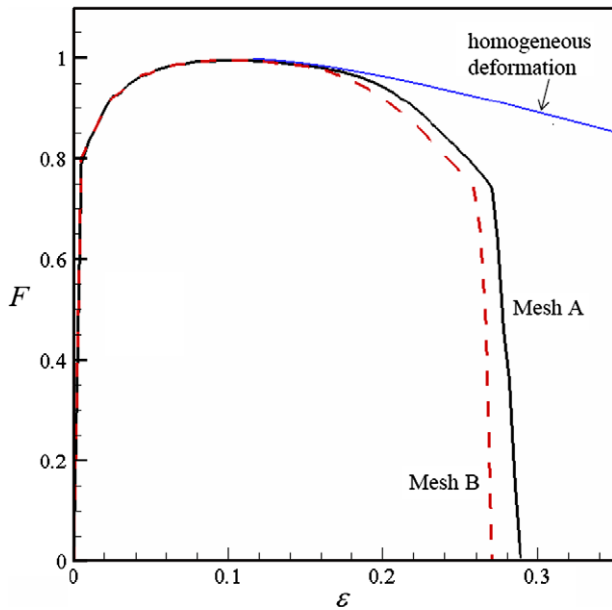
Fig. 7. Predicted applied force F and tensile strain $\varepsilon = \ln(1 + \Delta L/L_0)$ curve for the round bar under atmospheric pressure $(p = 0)$.
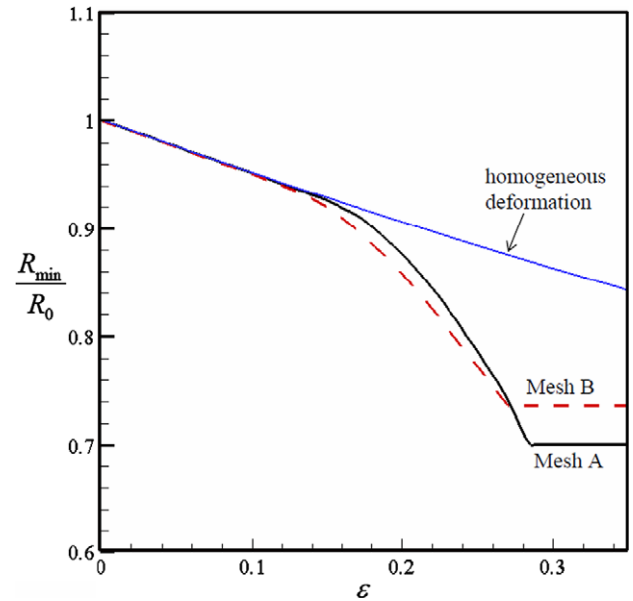

Fig. 8. Predicted normalized minimum radius (R_{min}/R_0) and tensile strain $\varepsilon = \ln(1 + \Delta L/L_0)$ curve for the round bar under atmospheric pressure $(p = 0)$.

based on the crude mesh (Mesh A). However, both meshes predict quite similar necking and fracture processes. The development of necking and failure processes can be more evidently presented in terms of the minimum cross-sectional area A_{min} vs. axial strain. For the axisymmetric problem considered here, $A_{min} = \pi R_{min}^2$ with R_{min} being the minimum radius in the necked region. Fig. 8 shows the calculated minimum radius and axial strain curve. Necking occurs where the curve deviates from that corresponding to the homogeneous tension. It is interesting to note that when fracture occurs, neck development essentially stops (R_{min} is almost a constant). As already pointed out by Tvergaard and Needleman (1984), this implies that the reduction in area at fracture is a representative measure of the onset of macroscopic fracture in the tensile test. Fig. 8 also indicates that both meshes predict quite similar necking and failure process with the finer mesh picking an earlier necking and failure.

Deformed meshes at various deformation stages are shown in Fig. 9. Since Mesh A will be used in the rest of the present paper, our explanations will mainly correspond to Mesh A with some

reference to Mesh B for the purpose of further assessing the mesh sensitivity. The predicted distributions of void volume fraction f at different deformation stages based on Mesh A are presented in Fig. 10. Using Mesh A, it is found that, at the axial strain around 0.270, fracture initiates at the centre of the neck, where the maximum stress triaxiality ($T = \sigma_H/\sigma_e$) is expected to occur. Due to the significant constraint resulting from the axisymmetry, the crack initially propagates almost vertically along the middle plane. This constraint becomes less and less with the distance from the centre of the neck. At an axial strain of 0.275, the crack has progressed about half way through the bar and tends to move away from the middle-plane and along the shear bands (though relatively weak and not clearly exhibited in Figs. 9 and 10). The evidence of the crack moving away from the middle-plane can be observed from the deformed meshes at an axial strain of about 0.264 based on Mesh B (Fig. 9). With further straining, the inclined crack has stopped and begins to zig-zag. The amplitude of the zig-zag increases as the crack approaches the free surface, where the axisymmetry constraint
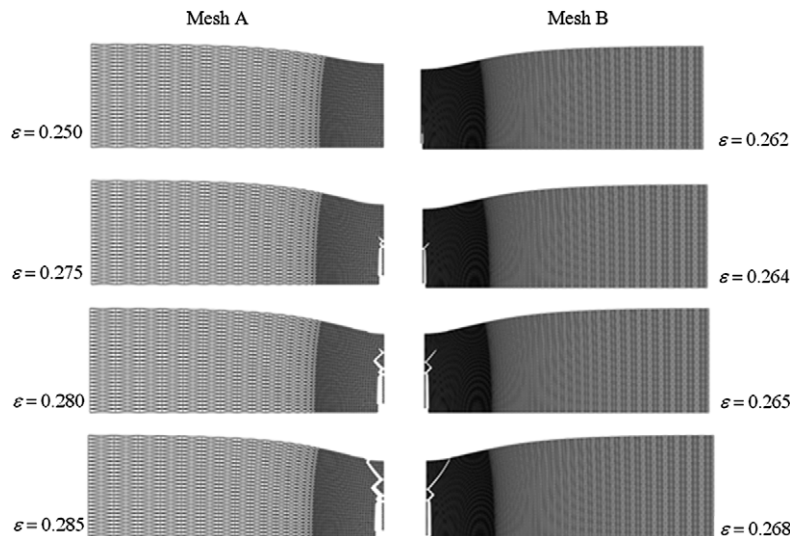

Fig. 9. Deformed meshes at various deformation stages for the round bar under atmospheric pressure $(p = 0)$.
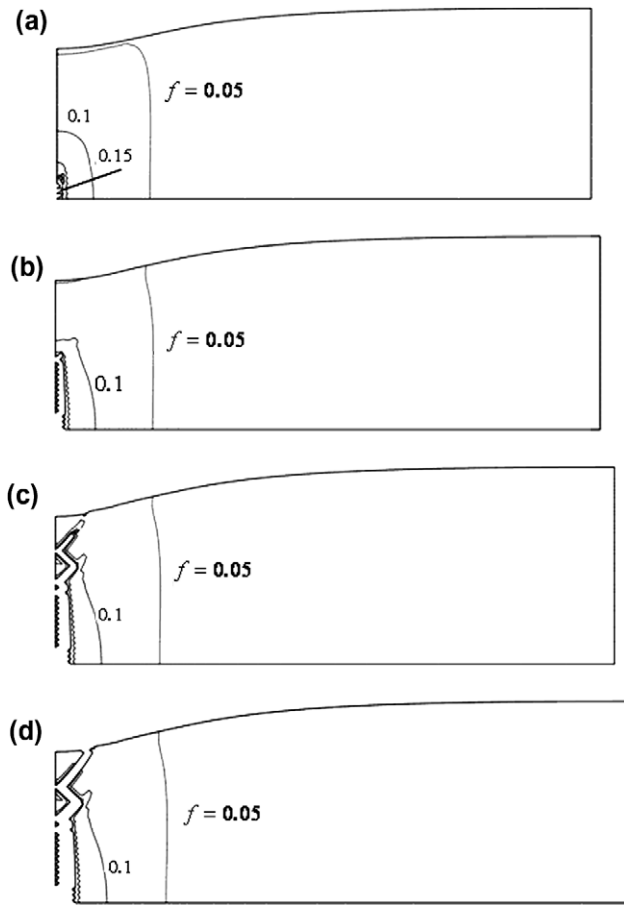
Fig. 10. Curves of constant void volume fraction at various stages for the round bar under atmospheric pressure. (a) $\varepsilon = 0.270$, (b) $\varepsilon = 0.274$, (c) $\varepsilon = 0.281$, and (d) $\varepsilon = 0.289$.

has been reduced significantly. This crack perturbation produces the cone of the cup-cone fracture surface. It is clear that both meshes are able to show the cup-cone fracture mechanism. The main difference between Mesh A and Mesh B is that the finer mesh detects fracture earlier and produces a relatively larger cone. Carefully examining the deformed meshes confirms that the initial zig-zag of the crack near the neck centre depicted in Fig. 13 of Tvergaard and Needleman (1984) was an artefact of the mesh they used. As mentioned by Tvergaard and Needleman (1984), it should be noted that the present study assumes symmetry about the middle-plane and thus two symmetrical conical fracture surfaces are predicted. However, in reality one of these cracks will finally dominate, which results in the cup-cone fracture observed experimentally (see also Besson et al., 2001).

Based on the above observations and the fact (which will become clear later) that the mesh sensitivity will be significantly reduced with an increase of the superimposed hydrostatic pressure, Mesh A will be used in the rest of the present paper although it is still crude in relation to the crack tip field. However, Mesh B was also applied in some cases, although not reported in the present paper, to further validate the numerical simulations.

We proceed by studying the effects of superimposed hydrostatic pressure $p = -\alpha\sigma_y$ on fracture in the round tensile bar. Fig. 11 shows the applied/measured tensile force $\overline{F}$ and axial strain ε curves. From Fig. 11, it is found that the hydrostatic pressure does not affect the maximum applied force point (the magnitude of the maximum force and the strain at which the maximum force is reached). However, the hydrostatic pressure clearly delays the sharp knee on the applied force vs. axial strain curve, and the
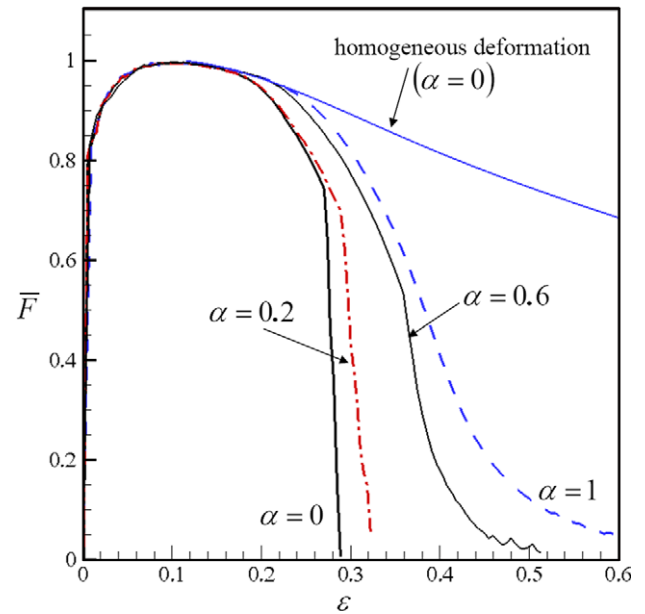

Fig. 11. Predicted *applied* force $\overline{F}$ and tensile strain $\varepsilon = \ln(1 + \Delta L/L_0)$ curves for the round bar under superimposed hydrostatic pressure $p = -\alpha\sigma_y$.

sharpness of the knee reduces significantly with increasing hydrostatic pressure. At high a pressure $(p = -\sigma_y)$ the knee disappeared and the applied force could decrease gradually to zero, which is consistent with the results reported by French and Weinrich (1975). Also from Fig. 11, it seems that the hydrostatic pressure has no noticeable effect on necking but only affects the deformation behavior after necking has started, which is consistent with most experimental findings (see e.g. French et al., 1973). As mentioned previously, the development of necking and failure can be very effectively assessed in terms of the calculated minimum radius vs. axial strain curve, which is now presented in Fig. 12. In the figure, the open circles represent the fracture initiation, while the solid squares indicate the completion of the fracture. It
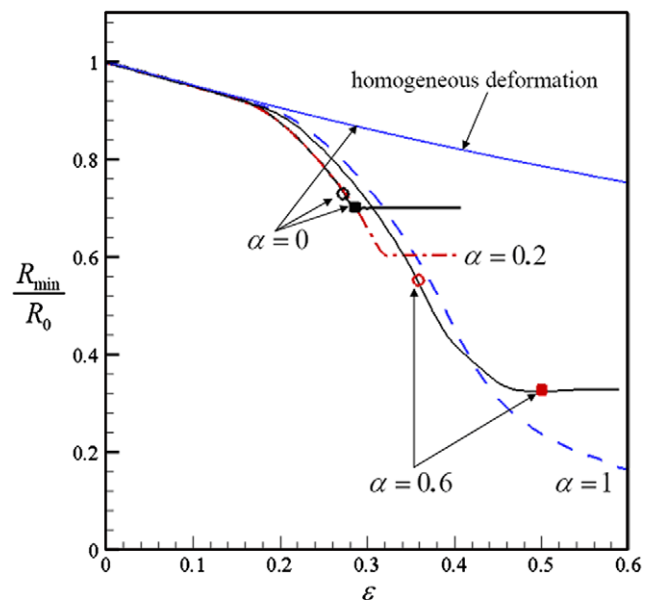

Fig. 12. Predicted normalized minimum radius (R_{min}/R_0) and tensile strain $\varepsilon = \ln(1 + \Delta L/L_0)$ curves for the round bar under superimposed hydrostatic pressure $p = -\alpha\sigma_y$. The open circles represent the fracture initiation, while the solid squares indicate the completion of the fracture.
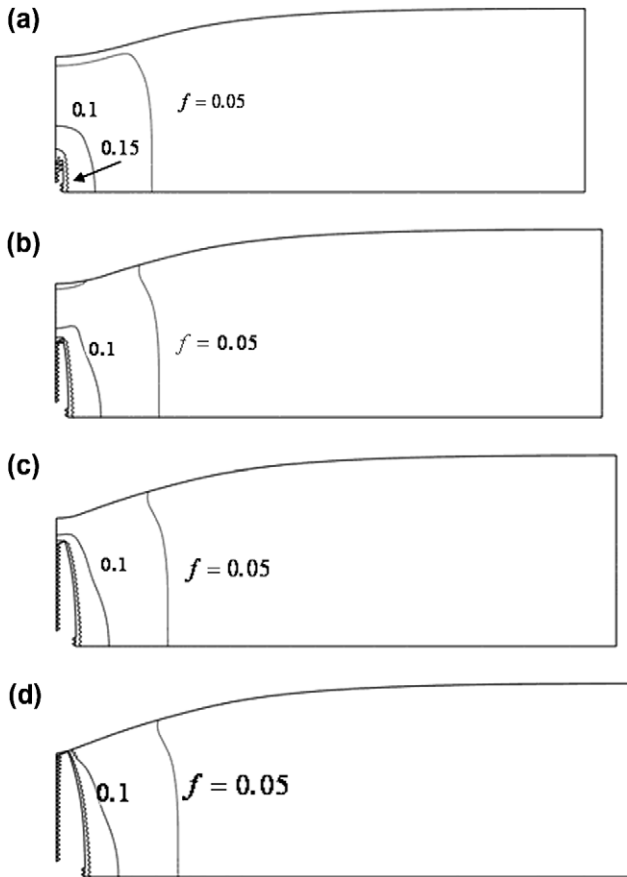
Fig. 13. Curves of constant void volume fraction at various stages for the round bar under superimposed hydrostatic pressure $p = -0.2\sigma_y$. (a) $\varepsilon = 0.292$, (b) $\varepsilon = 0.300$, (c) $\varepsilon = 0.311$, and (d) $\varepsilon = 0.326$.
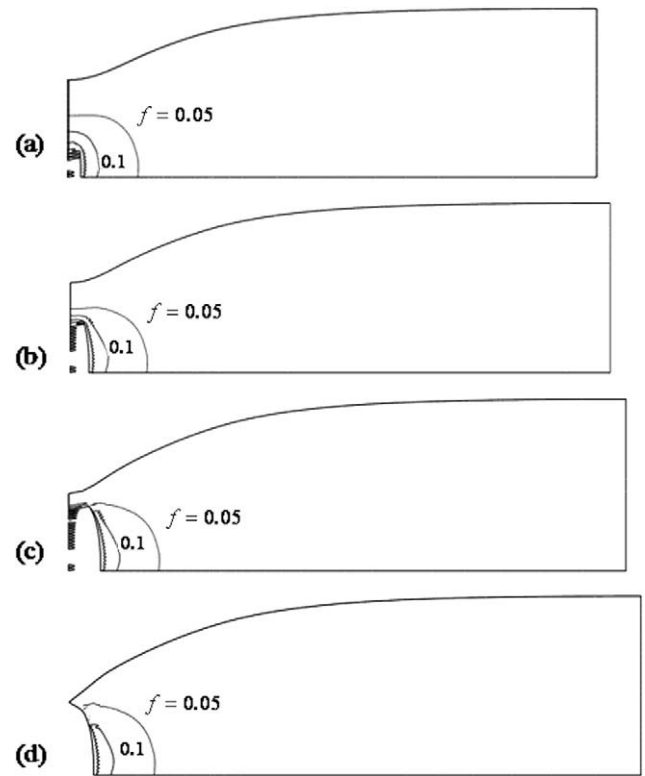

Fig. 14. Curves of constant void volume fraction at various stages for the round bar under superimposed hydrostatic pressure $p = -0.6\sigma_y$. (a) $\varepsilon = 0.364$, (b) $\varepsilon = 0.375$, (c) $\varepsilon = 0.397$, and (d) $\varepsilon = 0.429$.

becomes clear from Fig. 12 that the hydrostatic pressure has no noticeable effect on necking. It is also found that the reduction in area at completed failure increases significantly with increasing hydrostatic pressure. It is noted that without superimposed hydrostatic pressure fracture initiates at $\varepsilon = 0.270$ and the failure process is completed at 0.289. Under the hydrostatic pressure $p = -0.6\sigma_y$, these numbers become 0.356 and 0.519, respectively. Therefore, the superimposed hydrostatic pressure not only delays the initiation of cracking but also extends the failure process (from initiation of cracking to completely fracture).

Figs. 13 and 14 show the predicted distributions of void volume fraction under superimposed hydrostatic pressure $p = -0.2\sigma_y$ and $p = -0.6\sigma_y$, respectively. It is clear that a superimposed hydrostatic pressure makes a transition of the fracture surface from the cup-cone mode under atmospheric pressure (see Fig. 10) to smoother fracture surfaces under even relatively low pressures. The delay of fracture can be explained by showing how the superimposed hydrostatic pressure $p = -\alpha\sigma_y$ influences the hydrostatic stress $\sigma_H = \frac{1}{3}(\sigma_{zz} + \sigma_{rr} + \sigma_{\theta\theta})$ inside the necked region. Fig. 15 presents the hydrostatic/triaxial stress σ_H at the centre of the neck, where fracture initiates, as a function of axial strain ε at room pressure $p = 0$ and superimposed hydrostatic pressures $p = -0.2\sigma_y$ and $p = -0.4\sigma_y$. Fig. 15 also includes the calculated hydrostatic stress σ_H from the corresponding homogeneous deformations. For a given pressure, necking initiates where the curve deviates from the one that corresponds to homogeneous deformation. It is clear from Fig. 15 that in the range considered the superimposed hydrostatic pressure has no significant effect on necking. During tensile deformation at room pressure $p = 0$, the triaxial tensile stress

developed in the centre of neck is such as to assist the void growth. However, under a superimposed hydrostatic pressure $p = -\alpha\sigma_y$, the triaxial stress σ_H is initially compressive ($\sigma_H = p = -\alpha\sigma_y$). This implies that void nucleation and void growth are delayed until a sufficiently large tensile component of stress is introduced. As also mentioned by French et al. (1973), the greater the superimposed hydrostatic pressure the greater the degree of necking required to
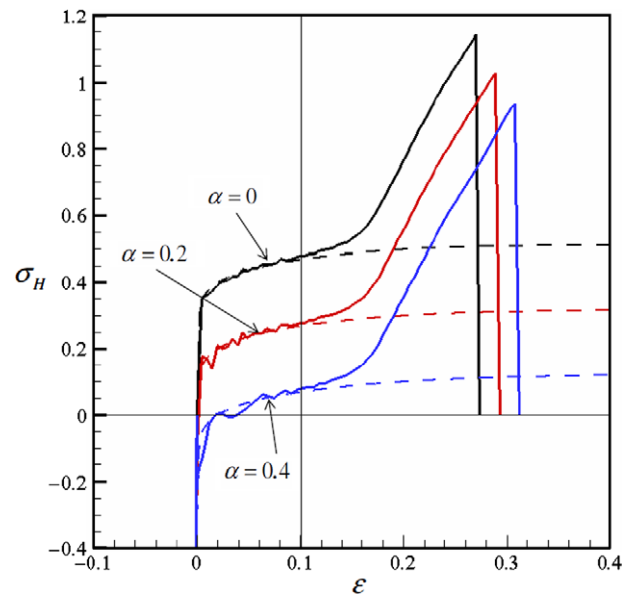

Fig. 15. Predicted hydrostatic stress σ_H at the centre of neck under superimposed hydrostatic pressure $p = -\alpha\sigma_y$. The dashed lines are those from the corresponding homogeneous deformations.
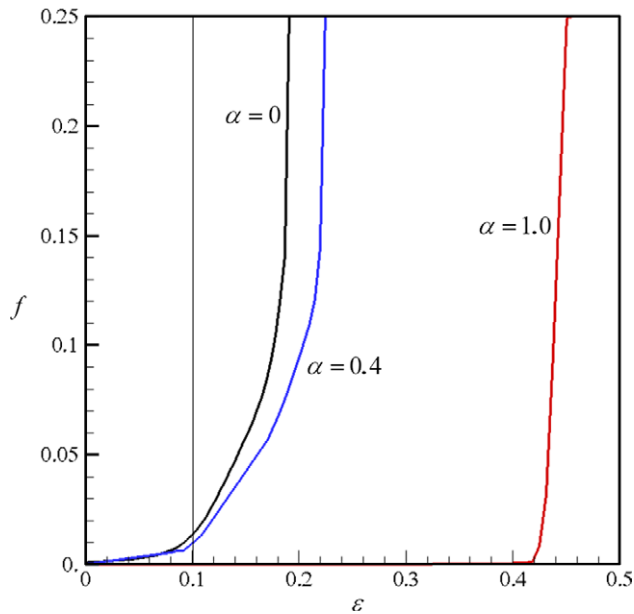
Fig. 16. Predicted void volume fraction f at the centre of neck under superimposed hydrostatic pressure $p = -\alpha\sigma_y$.

overcome the triaxial compressive stress at the centre of neck which counteracts the void nucleation and hence the greater the strain which can be withstood before fracture. Fig. 16 shows the predicted void volume fraction f at the centre of the neck under various superimposed hydrostatic pressures. It is clear that a superimposed pressure delays or could even completely eliminate the nucleation, growth and coalescence of voids. Figs. 15 and 16 also indicate that significant void growth has not occurred prior to necking. This is the reason for why a superimposed hydrostatic pressure has no noticeable effect on necking even for the porous materials described by the Gurson model.

Fig. 17 presents the calculated effect of superimposed hydrostatic pressure on the fracture strain ε_f. The fracture strain is defined as
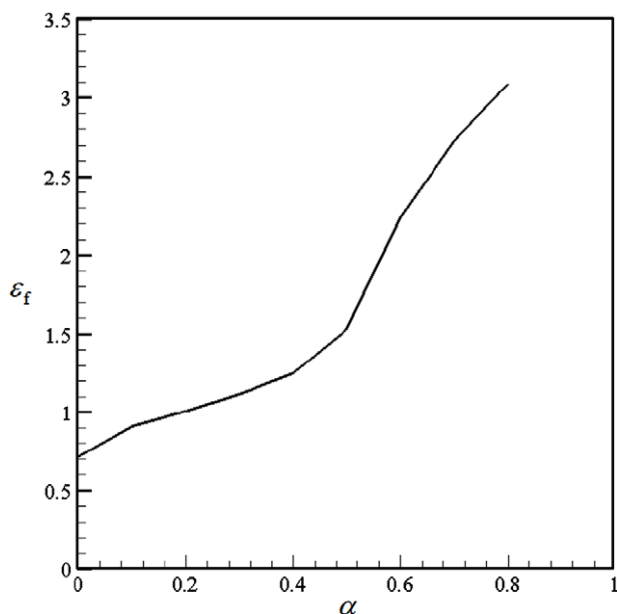

Fig. 17. Predicted effect of superimposed hydrostatic pressure $p = -\alpha\sigma_y$ on fracture strain ε_f.

$\varepsilon_f = \ln\left(\frac{A_0}{A_f}\right)$, where A_0 is the original cross-sectional area and A_f the final cross-sectional at the neck. It is found that the fracture strain increases with pressure nearly linearly at low pressures but at an increasing rate at high pressures. This is consistent with the results for cold worked copper reported by Li et al. (1964–1965). However, it should be pointed out that the predicted increase in ductility depends on the material and geometrical parameters used.

The mechanism of how a superimposed hydrostatic pressure could change the fracture surface from the cup-cone to a smoother surface is perhaps due to the fact that the superimposed pressure enhances the axisymmetry constraint. The greater the superimposed hydrostatic pressure, the greater the axisymmetry constraint reached inside the neck. Above a critical level of superimposed hydrostatic pressure, the axisymmetry constraint becomes so high that the initiated crack has to propagate along the middle-plane. It is expected that such a critical pressure level depends on geometrical and mechanical properties of the round tensile bar considered. By comparing Figs. 13 and 14 to Fig. 10, it is expected that under very high superimposed hydrostatic pressures the minimum radius R_{min} would approach zero.

5. Conclusions

In this paper, we have carried out a detailed finite element analysis of uniaxial tension under superimposed hydrostatic pressure. It has been demonstrated that, while a superimposed hydrostatic pressure has no noticeable effect on necking because significant void growth has not occurred prior to necking, the superimposed hydrostatic pressure significantly increases the fracture strain. This increment in ductility has been found to be due to the fact that a superimposed pressure delays or completely eliminates the nucleation, growth and coalescence of microvoids or microcracks. Numerical results have also indicated that a superimposed hydrostatic pressure changes the fracture surface from the cup-cone mode at room pressure to a slant structure under high pressure. It is important to keep in mind that while the significant increase in fracture strain is predicted with confidence, the calculated subtle change in appearance of fracture surface due to the superimposed hydrostatic pressure could be very sensitive to the mesh used and may even be an artefact of the mesh.

We have also numerically proved that a superimposed hydrostatic pressure has no effect on the necking strain for damage free round bars under axial tension. A Considère-type criterion based on the condition of $d\overline{F} = 0$ (rather than $dF = 0$) is appropriate to determine the onset of inhomogeneous deformation.

While we have studied the effect of superimposed hydrostatic pressure on fracture only in round tensile bars, experimental work has shown that a superimposed hydrostatic pressure increases the fracture strain under tension and enhances the bendability under bending in sheet metals (see e.g. Weinrich and French, 1976; Gimple et al., 2001; Kao et al., 1989). Numerical simulations of the effect of superimposed hydrostatic pressure on fracture in sheet metals are in progress and will be reported elsewhere.

Acknowledgments

References

Ashby, M.F., Embury, J.D., Cooksley, S.H., Teirlinck, D., 1985. Fracture maps with pressure as a variable. Scripta Metall. 19, 385–390.

Besson, J., Steglich, D., Brocks, W., 2001. Modeling of crack growth in round bars and plane strain specimens. Int. J. Solids Struct. 38, 8259–8284.

Bridgman, P.W., 1952. Studies in Large Plastic Flow and Fracture – With Special Emphasis on the Effects of Hydrostatic Pressure. McGraw-Hill, New York.

Brownrigg, A., Spitzig, W.A., Richmond, O., Teirlinck, D., Embury, J.D., 1983. The influence of hydrostatic pressure on the flow stress and ductility of a spheroidized 1045 steel. Acta Metall. 31, 1141–1150.

Carpentier, D., Contre, M., 1970. Description of an apparatus allowing mechanical tests under hydrostatic pressure up to 15 kilobars. Rev. Sci. Instrum. 41, 189–192.

Chen, B., Huang, Y., Liu, C., Wu, P.D., MacEwen, S.R., 2004. A dilatational plasticity theory for viscoplastic materials. Mech. Mater. 36, 679–689.

Chu, C.C., Needleman, A., 1980. Void nucleation effects in biaxially stretched sheets. J. Eng. Mater. Technol. 102, 249–256.

French, L.E., Weinrich, P.F., 1975. The influence of hydrostatic pressure on the tensile deformation and fracture of copper. Metall. Trans. A 6A, 785–790.

French, L.E., Weinrich, P.F., Weaver, C.W., 1973. Tensile fracture of free machining Brass as a function of hydrostatic pressure. Acta Metall. 21, 1045–1049.

Gimple, J.L., Wilkinson, D.S., Embury, J.D., Lewandowski, J.J., 2001. Effect of superimposed pressure on the fracture behaviour of aluminum automotive alloys. In: Das, S.K., Kaufman, J.G., Lienert, T.J. (Eds.), Aluminum 2001 – Proceedings of the TMS 2001, TMS, pp. 17–29.

Gurson, A., 1977. Continuum theory of ductile rupture by void nucleation and growth. Part I. Yield criteria and flow rules for porous ductile media. J. Eng. Mater. Technol. 99, 2–15.

Kao, A.S., Kuhn, H.A., Richmond, O., Spitzig, W.A., 1989. Workability of 1045 spheroidized steel under superimposed hydrostatic pressure. Metall. Trans. A 20A, 1735–1741.

Kao, A.S., Kuhn, H.A., Richmond, O., Spitzig, W.A., 1990. Tensile fracture and fractographic analysis of 1045 spheroidized steel under hydrostatic pressure. J. Mater. Res. 5, 83–91.

Korbel, A., Raghunathan, V.S., Teirlinck, D., Spitzig, W.A., Richmond, O., Embury, J.D., 1984. A structural study of the influence of pressure on shear band formation. Acta Metall. 32, 511–519.

Lewandowski, J.J., Lowhaphandu, P., 1998. Effects of hydrostatic pressure on mechanical behaviour and deformation processing of materials. Int. Mater. Rev. 43, 145–187.

Li, H., Pugh, D., Green, D., 1964–1965. The effect of hydrostatic pressure on the plastic deformation and fracture of metals. Proc. Inst. Mech. Eng. 179, 415–429.

Liu, D.S., Lewandowski, J.J., 1993. The effects of superimposed hydrostatic pressure on deformation and fracture. Part I. Monolithic 6061 aluminum. Metall. Trans. A 24A, 601–608.

Mear, M.E., Hutchinson, J.W., 1985. Influence of yield surface curvature on flow localization in dilatants plasticity. Mech. Mater. 4, 395–407.

Nahshon, K., Hutchinson, J.W., 2008. Modification of the Gurson model for shear failure. Eur. J. Mech. A 27, 1–17.

Sauer, J.A., Mears, D.R., Pae, K.D., 1970. Effects of hydrostatic pressure on the mechanical behaviour of polytetrafluoroethylene and polycarbonate. Eur. Polym. J. 6, 1015–1032.

Spitzig, W.A., Richmond, O., 1984. The effect of pressure on the flow stress of metals. Acta Metall. 32, 457–463.

Tvergaard, V., 1981. Influence of voids on shear band instabilities under plane strain conditions. Int. J. Fracture 17, 237–252.

Tvergaard, V., 1982. On localization in ductile materials containing spherical voids. Int. J. Fracture 18, 389–407.

Tvergaard, V., 1990. Material failure by void growth to coalescence. Adv. Appl. Mech. 27, 83–151.

Tvergaard, V., Needleman, A., 1984. Analysis of the cup-cone fracture in a round tensile bar. Acta Metall. 32, 157–169.

Weinrich, P.F., French, L.E., 1976. The influence of hydrostatic pressure on the fracture mechanisms of sheet tensile specimens of copper and brass. Acta Metall. 24, 317–322.

Wu, P.D., Embury, J.D., Lloyd, D.J., Huang, Y., Neale, K.W., 2009. Effects of superimposed hydrostatic pressure on sheet metal formability. Int. J. Plasticity 25, 1711–1725.